FRACTURE DETECTION AND CHARACTERIZATION

by

M. Nafi Toksöz and Fatih Güler

Earth Resources Laboratory
Department of Earth, Atmospheric, and Planetary Sciences
Massachusetts Institute of Technology
Cambridge, MA 02139

ABSTRACT

The effects of fractures on full waveform acoustic logs are studied on the basis of field observations, available theoretical models, and a series of ultrasonic laboratory experiments. Results from diffusion models applicable to fine microfractures and finite difference models of isolated fractures are reviewed. Laboratory experiments are carried out with fine microfractures around the borehole in a Lucite model, and isolated single fractures in aluminum models. Cases of horizontal and inclined (45°) fractures are studied as a function of fracture aperture and frequency of Stoneley waves. A vertical fracture model is also studied. Results indicate that the effect of different fractures are manifested differently on P, S, pseudo-Rayleigh, and Stoneley waves. Micro-fractures surrounding a borehole attenuate Stoneley waves most strongly. Vertical fractures attenuate Stoneley waves more strongly than other phases in the wave train. Horizontal and inclined fractures have a greater effect on P and S waves than on Stoneley waves.

INTRODUCTION

An important application of full waveform acoustic logging is the detection of open fractures and the determination of their hydraulic conductivities. Studies based on field data (Arditty and Staron, 1987; Paillet, 1983; Paillet et al., 1987; Hardin et al., 1987), theoretical modeling (Stephen, 1986; Mathieu and Toksöz, 1984, Tang and Cheng, this issue), and ultrasonic laboratory models (Güler and Toksöz, 1987; Lakey, 1985, Poeter, 1987) have been used to relate acoustic log characteristics to fracture properties. All studies show that full waveform acoustic logs are attenuated by fractures. The magnitudes of attenuation of different phases, such as the P, S, pseudo-Rayleigh, and Stoneley, have been different. Even for a given wave type, such as the Stoneley propagating across a fracture, the field results show complete attenuation in some cases and little attenuation in others. Theoretical results, obtained using different techniques

and different assumptions in formulating the problem, have yielded different results. Why are there such differences?

The purpose of this paper is to re-examine these results with the aid of new laboratory studies in order to provide a phenomenological explanation for acoustic wave attenuation across fractures. In the next section we review some field data and theoretical models. In the third section we present the new ultrasonic laboratory results.

FIELD OBSERVATIONS AND THEORETICAL PREDICTIONS

Field Data

Most field studies of fractures by full waveform acoustic logging have been conducted in crystalline rocks in the United States and Canada by a U.S.G.S. scientist (Paillet, 1983, Paillet et al., 1987) and in Europe and other parts of the world by Elf-Aquitaine investigators using E.V.A. (Arditty and Staron, 1987). The logging tools used in these two studies are quite different. U.S.G.S. logs were made with relatively high frequency tools, with frequency responsed peaked at greater than about 10 kHz. E.V.A. has a broadband response between about 2 and 15 kHz. To our knowledge, no benchmark field experiment with different full waveform acoustic tools has ever been carried out in the same borehole.

Figures 1a and 1b show iso-offset (2.1m spacing) plots of full waveform acoustic logs in Britton well #2 in Hamilton, Massachusetts. The well was drilled in crystalline rocks that are primarily granitic gneiss. The fracture zones in the borehole are well documented by conventional logs, temperature logs, a borehole acoustic televiewer, television and hydrophone surveys (Hardin and Toksöz, 1985). Some prominent fractures are clearly visible in Figures 1a and 1b at depths of 209, 212 and 290m. Compressional and shear head waves and pseudo-Rayleigh waves are significantly or completely attenuated at open fractures. Stoneley waves are not generated because of the large diameter (30 cm) of the borehole. Scattering of waves at a 209m fracture is observed, but at other fractures, significant scattering is not observed.

Another example of acoustic attenuation at fractures is shown in Figure 2. Data are from a well in crystalline rock in Mirror Lake, New Hampshire (Hardin et al., 1987). Various degrees of attenuation are seen at different fractures and identified by an acoustic televiewer. P and pseudo-Rayleigh waves are significantly attenuated. Stoneley wave attenuation appears to be less than that of the P wave.

Figure 3 shows an iso-offset section of E.V.A. logs from a borehole in crystalline rock in France (Mathieu and Toksöz, 1984). These broadband logs clearly show Stoneley waves with a frequency of about 2.5 kHz. The fracture completely attenuates P, S,

completely attenuated. This is the clearest evidence that Stoneley waves propagate across fractures more efficiently than P or pseudo-Rayleigh waves.

Theoretical Studies

There are three different studies of wave attenuation across fractures. The first is by Mathieu and Toksöz (1984). It treats the problem of Stoneley wave attenuation across a horizontal fracture as a function of fracture, aperture, frequency, formation and fluid properties. The problem is formulated with the assumption that attenuation results from reflection at a borehole-fracture intersection and as a result of fluid flow into the fracture. Scattering of Stoneley waves into other wave types are ignored. The attenuation mechanisms are schematically shown in Figure 4. The Stoneley wave attenuation A is defined by

$$A = 1 - \frac{P_T}{P_I}\,, \tag{0.1}$$

where P_I and P_T are incident and transmitted pressure amplitudes at a given frequency, respectively.

Attenuation as a function of fracture aperture, at three frequencies, is shown in Figure 5a, for a borehole with 3.8 cm radius. For the "slim" borehole, the frequency dependence is small, but the dependence on fracture aperture is strong. The theoretical curves for borehole radii of 5, 10 and 15 cm are shown in Figure 5b. Attenuation decreases with increasing borehole radius. The formation properties correspond to those of a crystalline rock with V_p = 5850 m/sec, V_s = 3350 m/sec, and ρ = 2.65 g/sec. The fluid is water. Note that although the figures show attenuation as a function of fracture aperture, the important parameter is the hydraulic conductivity or transmissivity (T) which is related to permeability (K) and fracture aperture (L) by

$$T = K \cdot L\,. \tag{0.2}$$

Furthermore, it is assumed that flow is laminar and governed by Darcy's Law; cubic law for flow in fractures applies (Snow, 1965; Van Golf-Racht, 1982). With these assumptions, transmissivity (T), fracture aperture (L) and fluid parameters are related by (Paillet et al., 1987)

$$T = \frac{\rho_f \cdot g L^3}{12\mu}\,, \tag{0.3}$$

where ρ_f = fluid density, g = acceleration of gravity, and μ = fluid viscosity. Thus, in Figures 5a and 5b the fracture aperture can be converted to equivalent transmissivity or permeability.

It is important to keep in mind that the nature of assumptions limit the application of attenuation curves given in Figures 5a and 5b to cases where Darcy flow apply—small

aperture fractures. In addition, since wave scattering is neglected, the model cannot be applied to large fractures. Paillet and Hess (1986) and Paillet et al. (1987) found that the Mathieu model gave good results when applied to multiple and fine fractures. Figure 6 shows the theoretical attenuation curves as a function of fracture permeability, in a model where the fractured zone contains 100 to 2,000 fine fractures per meter. In this case the assumptions involved in theoretical formulations are satisfied. The curves show that if permeability of the zone is 10 darcy, the high frequency tube waves are almost completely attenuated over a 2-foot interval.

A more complete model of Stoneley wave attenuation across a horizontal fracture is presented in a paper by Tang and Cheng in this report. The basic assumptions are similar to those of Mathieu and Toksöz, except propagation effects along the fracture are taken into account along with the viscous flow effects. The result is a model that is similar to the Mathieu and Toksöz model at low frequencies and high viscosities, but have larger dependence on frequency, fracture aperture, and viscosity. Tang and Cheng were able to fit the model to the data of Poeter (1987).

The attenuation of full waveforms crossing an isolated horizontal fracture was calculated by Stephen (1986) using the finite difference approach. The model is perfectly elastic, without intrinsic attenuation. Neither Biot nor Darcy type flow is included in the calculations. Figures 7a and 7b show synthetic full waveform acoustic logs for a vertically homogeneous sandstone and for the same sandstone with 1 cm thick horizontal fracture. The fracture attenuates P, pseudo-Rayleigh, and Stoneley waves at 15 kHz by about a factor of 2; Stoneley attenuation is less that that of P. There is an observable Stoneley wave reflected from the fracture. Frequency dependence of attenuation and complex scattering can be observed by comparing Figures 7a and 7b. Clearly in the case of isolated major fractures, numerical solutions are required to understand scattering and attenuation. At the present time, these calculations can be done only for horizontal fractures. Also, numerical codes for very thin fractures and those that incorporate fluid flow, need to be developed. The laboratory models discussed in the next section provide a physical insight into such cases.

LABORATORY MODELS OF FRACTURES

Laboratory modeling of acoustic wave propagation in a borehole complements the theoretical studies for the understanding and interpretation of field data. In this section we describe the ultrasonic laboratory results of the effects of fractures on full waveform acoustic logs. There are few papers on laboratory studies of full waveform acoustic logs in a borehole (Chen, 1982; Lakey, 1985; Shortt, 1986; Güler and Toksöz, 1987, Poeter, 1987). Except for Güler and Toksöz (1987), none of these addresses the problem of vertical fractures. One difficulty of laboratory work is the complexity of experiments, particularly adequate scaling of physical dimensions and wavelengths.

The second problem arises from the complexity of waveform microseismograms which require sophisticated analysis for the identification of wave types and interpretation of the results.

Two separate experiments are carried out. The first studies the effects of microcracks around the borehole. The second studies the isolated single fractures that are horizontal, inclined (45°), or vertical. Wavelength scaling is used to determine the physical dimensions of the model, including the borehole radius. The frequency response of the source-receiver transducers covers a range of 30 kHz to 600 kHz. The modeling materials are Lucite and aluminum. The borehole diameter is 1 cm. With these specifications, the aluminum model corresponds to a 2 to 30 kHz frequency band in the field with a 20 cm (8") diameter borehole. The data are collected with a fixed source and a moving receiver.

Lucite and aluminum with a diameter of 20 cm (8") and a length of 30 cm (12") are used for the experiments. Each cylinder is center drilled and reamed to produce a smooth 1 cm diameter borehole. Full waveform experiments are performed before fractures are introduced, and repeated with fractures. The experimental set-up and procedures are described in detail in an earlier paper (Güler and Toksöz, 1987).

Microfractures Around the Borehole

The first set of experiments investigate the effects of microfractures on the attenuation of full waveform acoustic logs. Lucite cylinder was used for the experiments. After the borehole was drilled, the first data set was collected. In the following weeks small microcracks developed around the borehole due to stress relaxation. There were horizontal, vertical, and inclined fractures with characteristic dimensions of millimeters. Fracture density decreased away from the borehole and no fractures extended more than 10 mm beyond the borehole wall. In one region there was a predominant vertical fracture. In others, orientations appeared to be random. The borehole remained smooth and intact, and no material fell from the wall. A schematic diagram of the cylinders is shown in Figure 8, before the fractures formed and after.

The full waveform microseismograms are shown in Figure 9 for the crack-free and cracked cases. To the left (Figures 9a and 9c) are broadband microseismograms, and to the right (Figures 9b and 9d) are the filtered waveforms showing the Stoneley waves. The P velocity in Lucite is 2.4 km/sec and the S velocity is 1.4 km/sec, slightly less than sound velocity in water. In Figure 9a, P waves, P leaky modes, and Stoneley waves are visible. The small pulse at about 80 μ/sec is the P wave reflected from the outer surface of the cylinder.

To separate the Stoneley waves, we use a pie-slice or fan filter in the f-k domain. Especially in the later experiments, where there is an overlap in time between Stoneley

and pseudo-Rayleigh, the fan filtering is more effective than low-pass or band-pass filtering. In the f-k domain, both the individual modes and the frequency band where a given mode has adequate power, is separated. To look at different frequency bands, both fan- and band-pass filtering are used.

The Stoneley waves shown in Figure 9b are attenuated. The Q value calculated is 25 and close to the shear wave Q of Lucite. The group velocity of Stoneley waves is about 1.0 km/sec and there is no significant dispersion in this frequency range.

Figures 9c and 9d show the results from a model with microcracks. Crack density is not uniform along the borehole. In the 10 to 30 mm distance range, there is a prominent vertical fracture. Randomly oriented fractures dominate a 30 to 80 mm distance range. The attenuation of all phases are clearly shown. The Stoneley waves are dispersed and strongly attenuated. Since we could not measure fracture apertures or permeability, we cannot determine how much of the attenuation is due to fluid flow versus increased shear wave attenuation in microfractured zone. Note that P waves and high frequency P leaky modes are visible, and they are attenuated less than the low-frequency Stoneley waves. We judge that fluid flow plays a major role in the Stoneley wave attenuation.

Isolated Fractures

Three types of single fractures—horizontal, inclined at 45°, and vertical—were studied. Geometries are shown schematically in Figure 10. Aluminum cylinders, 20 cm in diameter and 30 cm long, with 1 cm diameter borehole were used. For horizontal and inclined fracture cases, the block was sawn in two after the initial measurements. For vertical fractures, a 1 mm sew-cut was make parallel to the axis, dissecting the borehole and the block. The vertical extent of the fracture was 15 cm.

For horizontal and inclined fractures, measurements were made with different fracture apertures, ranging from 0.2 mm to 4.5 mm. The source-receiver spacing was increased from 2 to 86 mm, at 2 mm increments. The fracture was centered at about 38 mm. In each case the broadband microseismograms were recordered. Different wave types were identified in the f-k domain. Stoneley waves were separated by fan filtering. Attenuation at different frequency bands was determined from band-passed and fan-filtered microseismograms. Frequency bands were determined from the f-k spectra. For vertical fractures, measurements were made for one aperture equal to 1.00 mm. The results for each case are discussed below.

Horizontal Fractures

Measurements were made with fracture apertures of 0.2, 0.5, 1.0, 2.5, and 4.5 mm. The thinnest fracture case corresponds to aluminum blocks sitting on top of each other held apart by the roughness of the polished surfaces and a layer of water. In other cases the blocks were separated by shims to obtain the desired aperture. The broadband microseismograms are shown in Figure 11, for four apertures. In addition to P, S, and Stoneley, several modes of pseudo-Rayleigh waves are recorded. Attenuation and scattering of different waves, as a function of fracture aperture are indicated. The Stoneley waves, separated by f-k filtering, are shown in Figure 12. As fracture aperture increases, so does the reflection from the fracture. Broadband and filtered microseismograms for the 0.5 mm wide fracture case are shown in Figure 13. Note that the Stoneley attenuation is substantial in this case.

To analyze the effects of fracture on Stoneley waves, the rms amplitude is plotted as a function of source receiver separation for three frequency bands centered at 50, 85, and 135 kHz. Since there is no geometric spreading and insignificant attenuation in water and aluminum, if it were not for the fracture, Stoneley amplitudes would be constant as a function of distance. Figure 14 shows the amplitude plots. There are three major observations:

1. Attenuation is greatest at lowest frequency and least at highest frequency.
2. At low and intermediate frequencies, attenuation increases from 0.2 mm to 0.5 mm fracture aperture, decreases at 1.0 mm, and then increases again at 2.5 mm and 4.5 mm.
3. As the fracture is approached, the Stoneley amplitudes oscillate and generally increase before the fracture. This last observation can be explained by the interference of the incident and reflected waves as the receiver approaches the fracture.

The first observation is consistent with the model of Mathieu and Toksöz and that of Tang and Cheng. The second observation points out the fact that Stoneley wave attenuation across a fracture cannot be explained by fluid flow alone. Scattering from the fracture has to be taken into account. At large apertures and relatively high frequencies, the viscous effect becomes minimal and attenuation across a fracture is due primarily to the scattering from the fracture and wave propagation along the fracture away from the borehole. Comparing the microseismograms (Figure 13) and amplitudes (Figure 14) with the finite difference synthetics (Figure 7b) shows similar amplitude decrease across the fracture, although the latter ignores viscous effects. In experiments, P wave amplitudes decrease more than those of model calculations, and this may be due to greater impedance contrast between aluminum and water than between the sandstone and water used in finite difference models.

The decrease of attenuation as a function of increasing frequency of Stoneley waves can be attributed to the borehole diameter to wavelength ratio. At a short wavelength the borehole acts like a finite piston. The Stoneley pulse propagates across the aperture with little or no disturbance and couples to the borehole on the other side. At long wavelengths, the end of the borehole acts like a point source. Although these arguments are qualitative, physically they are consistent with observations.

Inclined Fractures

The broadband microseismograms for 45°inclined fractures are shown in Figure 15 for four fracture apertures—0.0, 1.0, 2.5, and 4.5 mm. Attenuation increases with increasing fracture aperture. Also, the zone of attenuation is broadened because of the fracture inclination. The f-k filtered Stoneley waves are shown in Figure 16. No reflections are observed from the attenuation appear to be more significant than the horizontal fracture case. The Stoneley amplitudes as a function of distnace, at three frequency bands are shown in Figure 17. There is no attenuation across the 0.0 mm fracture. In this case the surfaces were machined and polished to obtain greater smoothness than the horizontal case. Attenuation is greater at low and intermediate frequencies than at high frequencies. Amplitude decrease is spread to a wider depth zone than the horizontal fracture case. There is a decrease in attenuation as fracture aperture increases from 1.0 mm to 2.5 mm.

The Stoneley attenuation as a function of fracture width and frequency is shown in Figure 18 for horizontal and inclined fractures. In both cases attenuation is greater at lower frequencies. The increase of attenuation with increasing fracture width is similar in both cases. At the lowest frequency, the horizontal fracture attenuates the Stoneley waves more than the inclined fracture. Both sets of measurements suggest a dual mechanism for attenuation. In the case of very thin fractures ($L \leq 1.0$ mm), fluid flow may play a significant role. In the case of thicker fractures, scattering is the primary mechanism of attenuation.

Vertical Fractures

Broadband and f-k filtered microseismograms for a borehole with a vertical fracture 1 mm wide are shown in Figures 19a and 19b, respectively. The broadband microseismograms show the attenuation and scattering of waves. P wave attenuation is slight. There is an S to P scattering at the fracture tip. The high frequency components of pseudo-Rayleigh waves are not attenuated significantly. In fact, they may increase due to Stoneley to pseudo-Rayleigh scattering. The Stoneley waves attenuate slowly once they encounter the fracture and propagate in the fractured section. There are no observable reflections.

Amplitudes of P, S, pseudo-Rayleigh, and Stoneley waves as a function of increasing distance are shown in Figure 20. Stoneley attenuation in the fractured zone is significant. The S attenuation increases in the fractured zone, most likely due to scattering. P wave attenuation is slight; pseudo-Rayleigh shows no attenuation. In fact, its rms amplitude increases possibly due to energy scattering into this mode.

The frequency dependence of Stoneley attenuation along the vertical fracture is shown in Figure 21. Attenuation is greatest at the lowest and decreases with increasing frequency.

CONCLUSIONS

The detection and characterization of fractures by full waveform acoustic logs requires a multifaceted approach, including field data, theoretical modeling and laboratory studies. Based on the available theoretical models and ultraosnic laboratory studies, we conclude that the effects of fractures on full waveform logs depend upon: (1) whether fractures are single, isolated with apertures of millimeters or greater, or a series of microfractures that intersect the borehole; (2) on the attitude (horizontal, inclined, or vertical) of the fracture plane; (3) on the wave type (P, S, pseudo-Rayleigh, or Stoneley); and (4) on frequency. Fluid flow and wave scattering play major roles in affecting the full waveform logs.

In the case of microfractures, Stoneley waves are strongly attenuated while other phases in the wave train are less attenuated. In the cases of horizontal or inclined isolate fractures, P and S waves are attenuated more strongly by the fracture. Stoneley attenuation decreases with increasing frequency. In the case of vertical fractures, Stoneley waves are attenuated more strongly than P or pseudo-Rayleigh waves. Again, Stoneley attenuation is greater at lower frequencies.

ACKNOWLEDGEMENTS

This research was supported by the Full Waveform Acoustic Logging Consortium at M.I.T.

REFERENCES

Arditty, P.C. and Staron, P., Lithologic analysis and fracture detection for EVA data: Examples in open and cased holes, Sonic Fullwave Research Workshop, *Soc. Expl. Geophys. 57th Ann. Mtg.,* New Orleans, 1987.

Chen, S.T., the full acoustic wave train in a laboratory model of a borehole, *geophysics, 47,* 1512–1520, 1982.

Güler, F. and Toksöz, M.N., Ultrasonic laboratory study of full waveform acoustic logs in boreholes with fractures, *M.I.T. Full Waveform Acoustic Logging Consortium Annual Report,* 511–530, 1987.

Hardin, E.L. and Toksöz, M.N., Detection and characterization of fractures from generation of tube waves, *Trans. SPWLA 26th Ann. Logging Symp.,* Paper II, 1985.

Hardin, E.L., Cheng, C.H., Paillet, F.L., and Mendelson, J.D. Fracture characterization by means of attenuation and generation of tube waves in fractured crystalline rock at Mirror Lake, New Hampshire, *J. Geophys. Res., 92,* 7989–8006, 1987.

Lakey, K.G., Physical modeling of the full acoustic wave train in a borehole with a perpendicular fracture, M.S. thesis, Washington State University, Pullman, Washington, 1985.

Mathieu, F. and Toksöz, M.N., Application of full waveform acoustic logging data to the estimation of reservoir permeability, *Proc. Soc. Expl. Geophys., 54th Ann. Int. Mtg.,* Atlanta, Georgia, 9–12, 1984.

Paillet, F.L., Acoustic characterization of fracture permeability at Chalk River, Ontario, Canada, *Geotech. J., 20,* 468–476, 1983.

Paillet, F.L. and Hess, A.E., Geophysical well log analysis of fractured crystalline rocks at East Bull Lake, Ontario, Canada, U.S. Geological Survey Water Resources Investigations Report 86-4052, 1986.

Paillet, F.L., Hess, A.E., Cheng, C.H., and Hardin, E.L., Characterization of fracture permeability with high-resolution vertical flow measurements during borehole pumping, *Ground Water, 25,* 28–40, 1987.

Poeter, E.P., Characterizing fractures at potential nuclear waste repository sites with acoustic waveform logs, *The Log Analyst, 28,* 453–461, 1987.

Shortt, E.R., Laboratory borehole model, *M.I.T. Full Waveform Acoustic Logging Consortium Annual Report,* 461–470, 1986.

Snow, D.T., A parallel plate model of fractured permeable media, Ph.D. thesis, Uni-

versity of California, Berkeley, 1965.

Stephen, R.A., Synthetic acoustic logs over bed boundaries and horizontal fissures, *M.I.T. Full Waveform Acoustic Logging Consortium Annual Report,* 365–414, 1986.

Tang, X.M. and Cheng, C.H., A dynamic model for fluid flow in a borehole fracture, *M.I.T. Full Waveform Acoustic Logging Consortium Annual Report,* 87–104, 1988.

Van Golf-Racht, T.D., *Fundamentals of fractured reservoir engineering,* Elsevier, Holland, 1982.

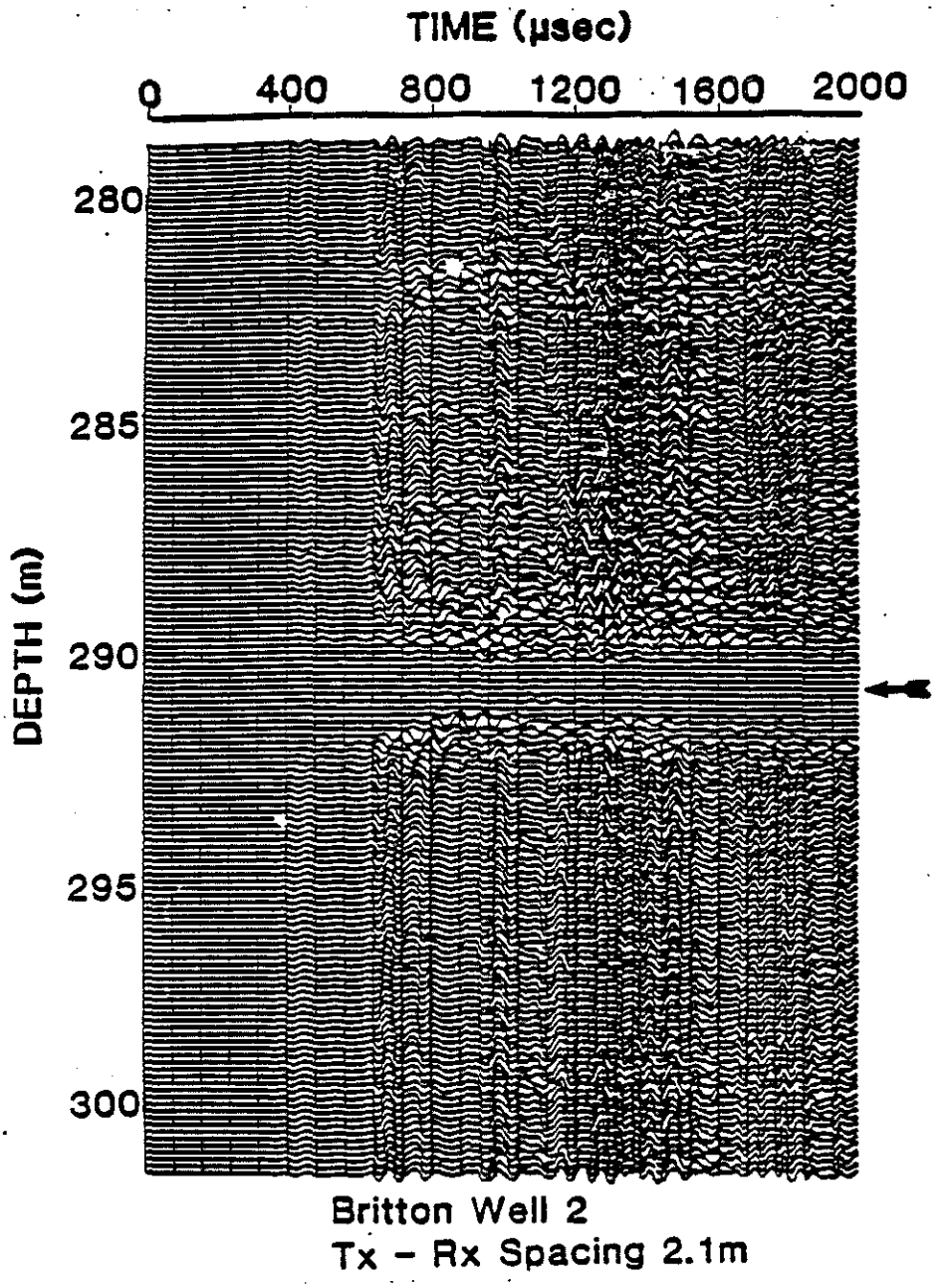

Figure 1a: Full waveform acoustic log traces from an interval encompassing the tube wave generating horizon at 210m.

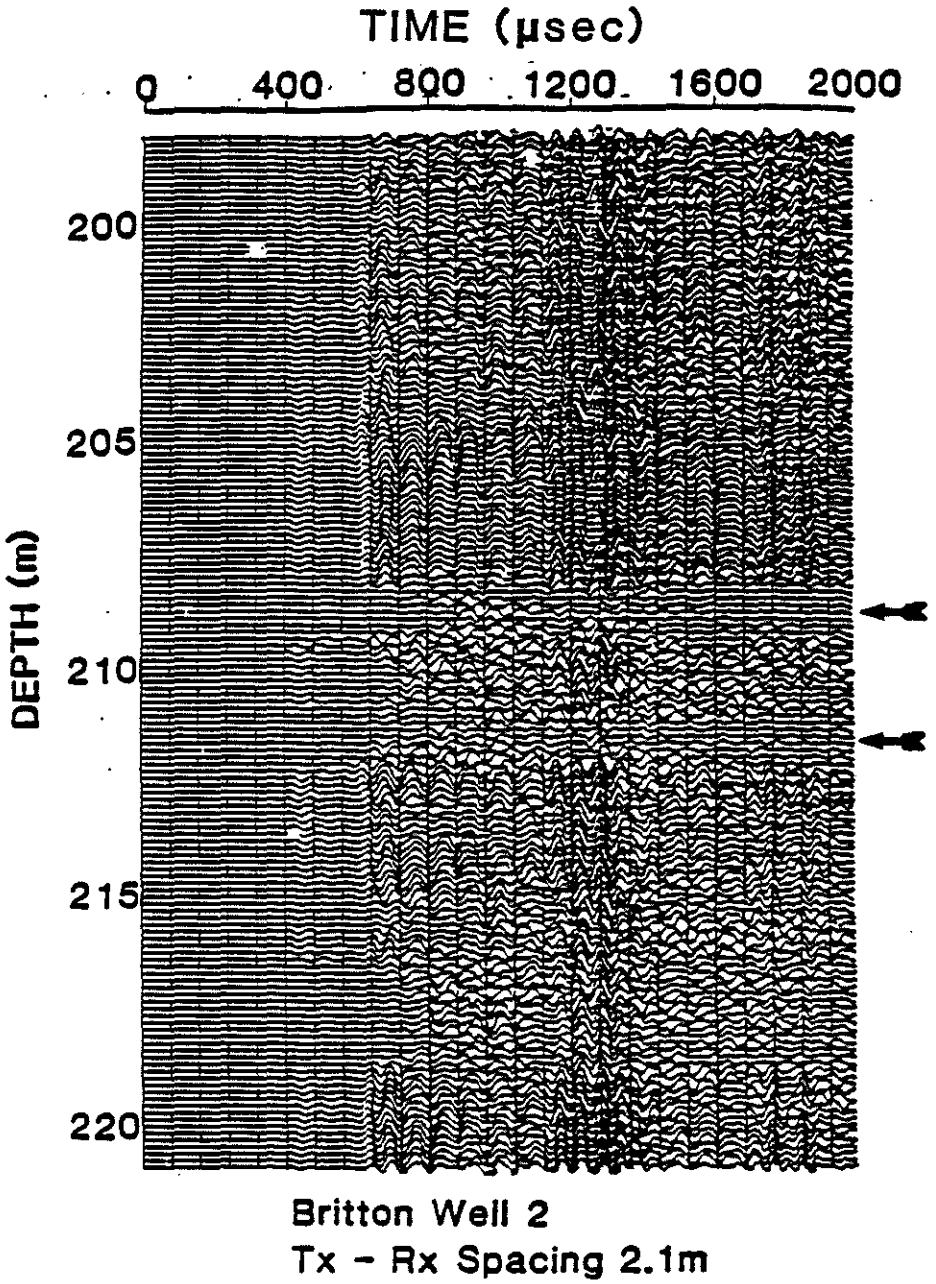

Figure 1b: Full waveform acoustic log traces from an interval encompassing the tube wave generating horizon at 290m.

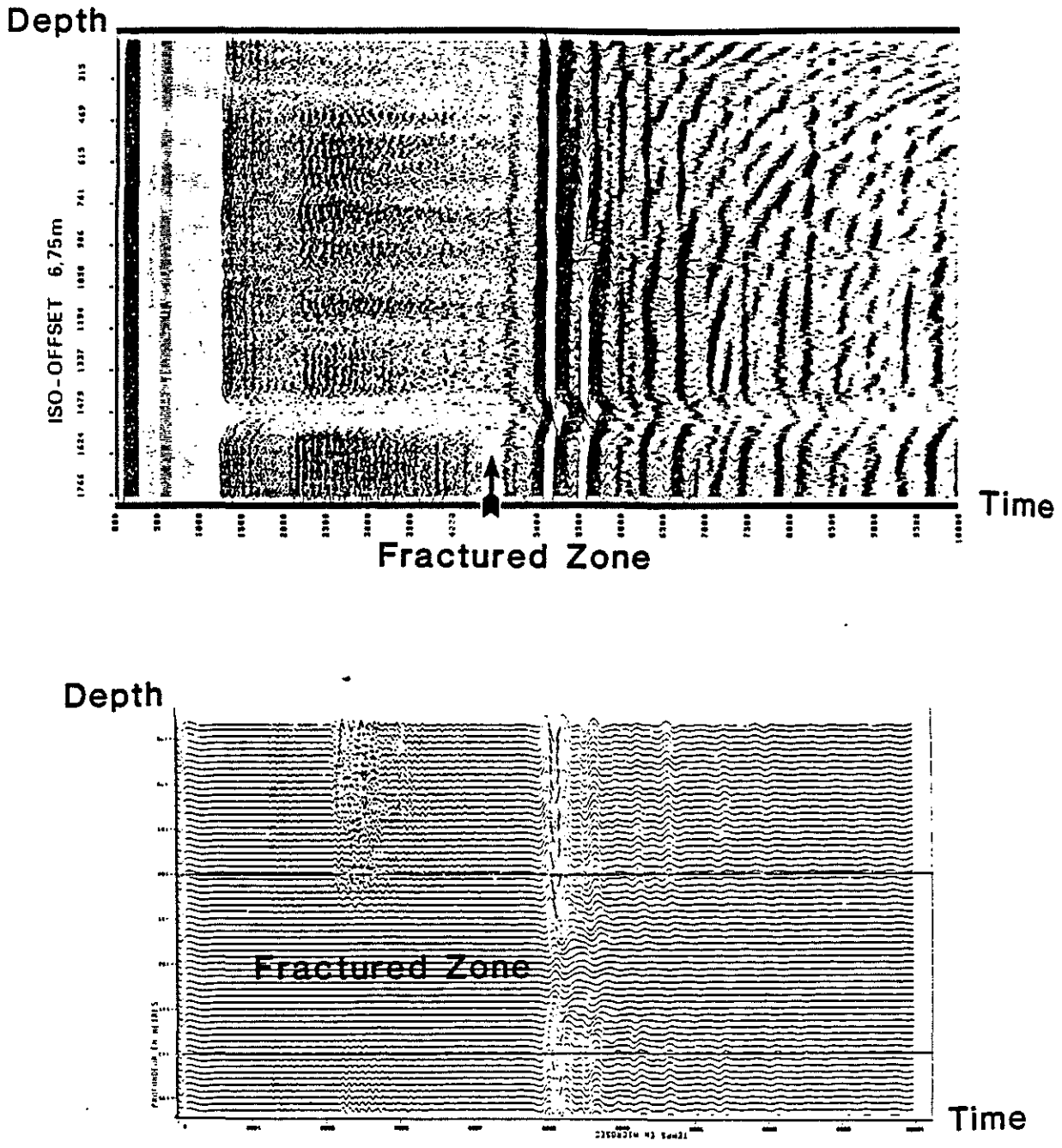

Figure 2: Full waveform acoustic data recorded after a hydrofracturing experiment.

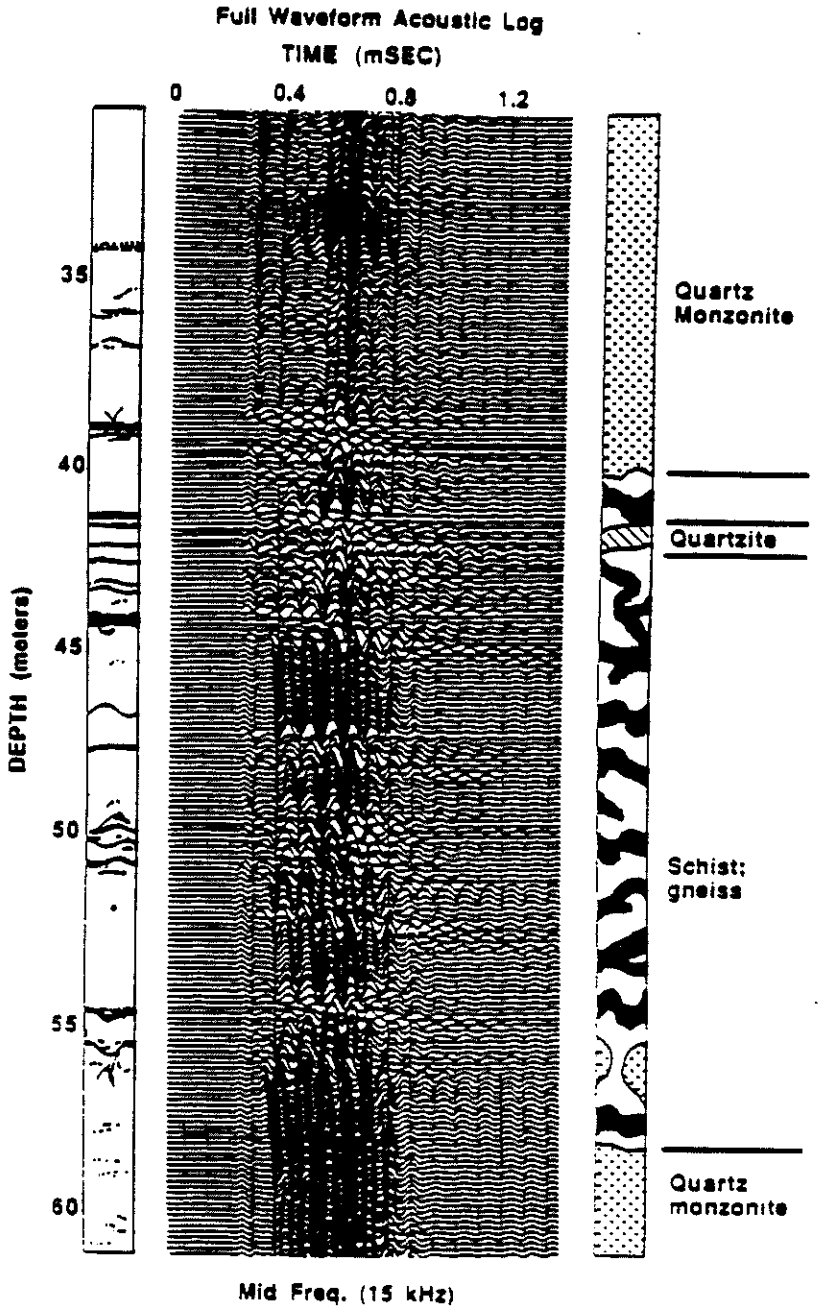

Figure 3: Full waveform acoustic log from EBR-4 Mirror Lake well, interval from 30 to 60 meters containing tube wave generating horizon at 44 meters. Separation: 0.91 meters, approx. source band center frequency: 15 kHz. Stoneley packet can be distinguished from pseudo-Rayleigh, although not at every depth.

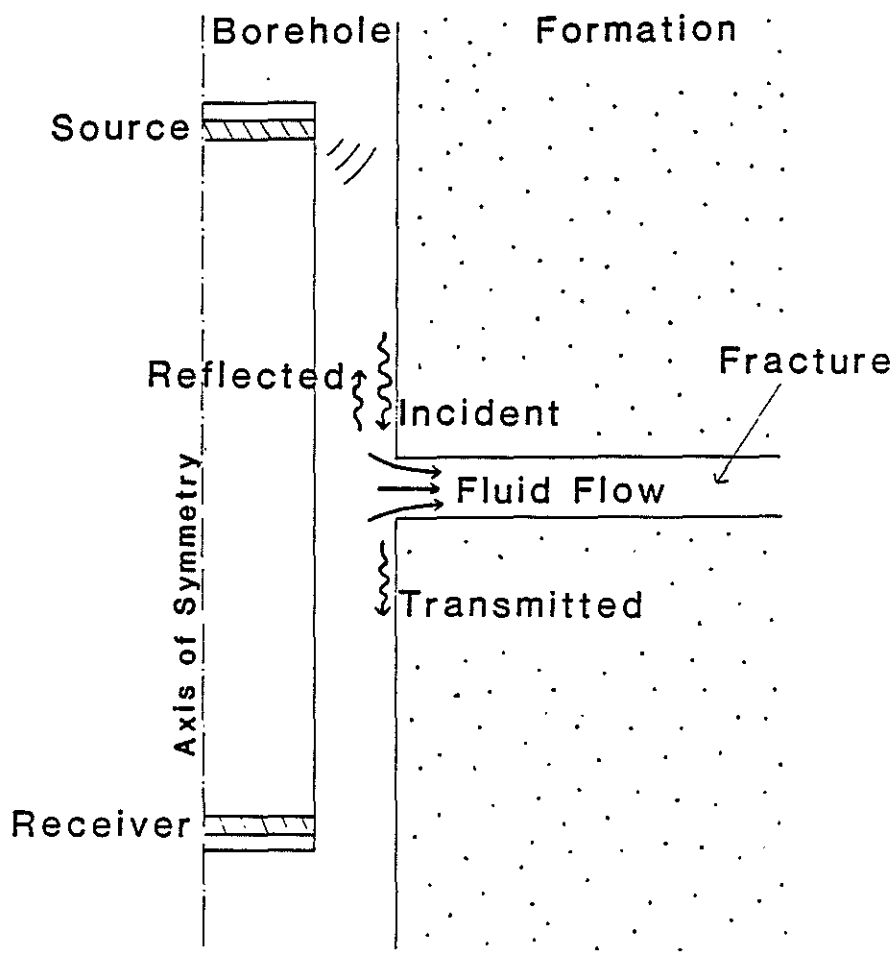

Figure 4: Schematic diagram of the attenuation mechanism in the case of a single fracture.

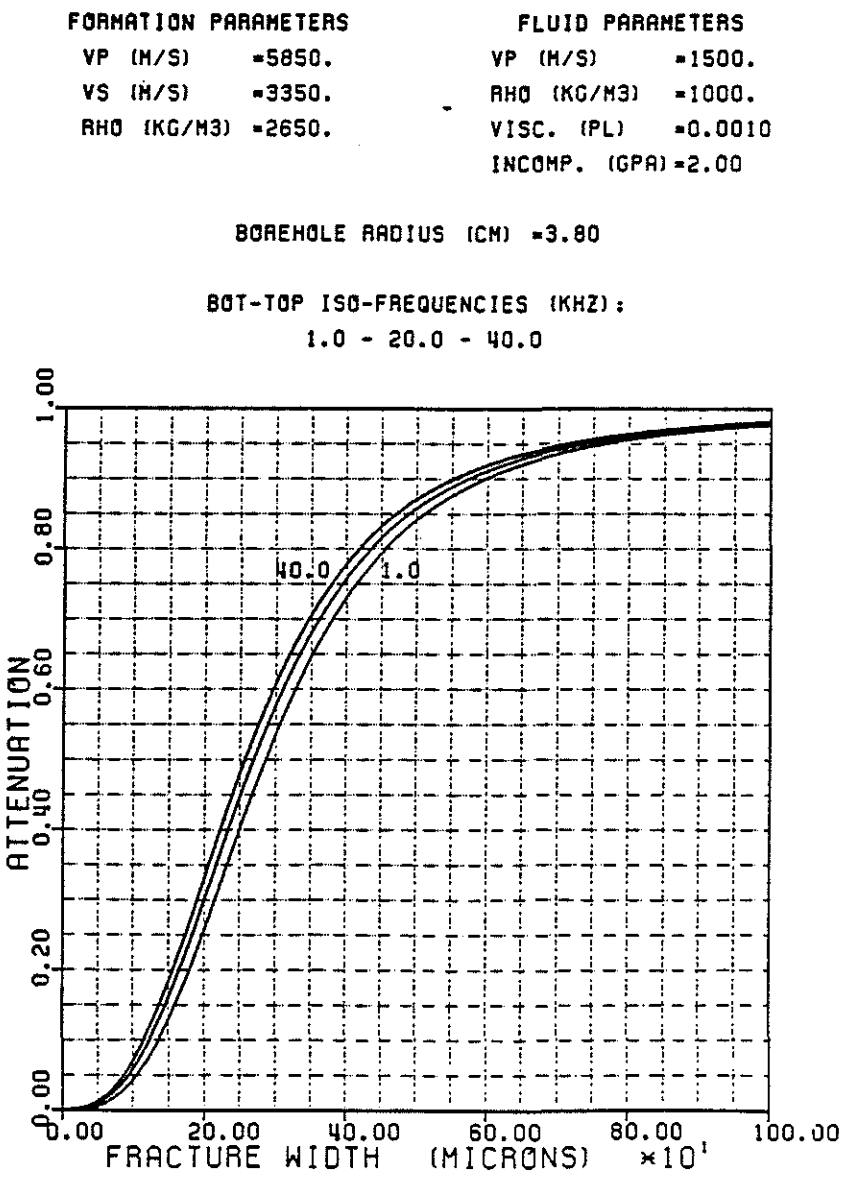

Figure 5a: Frequency effect on attenuation in the case of a single fracture.

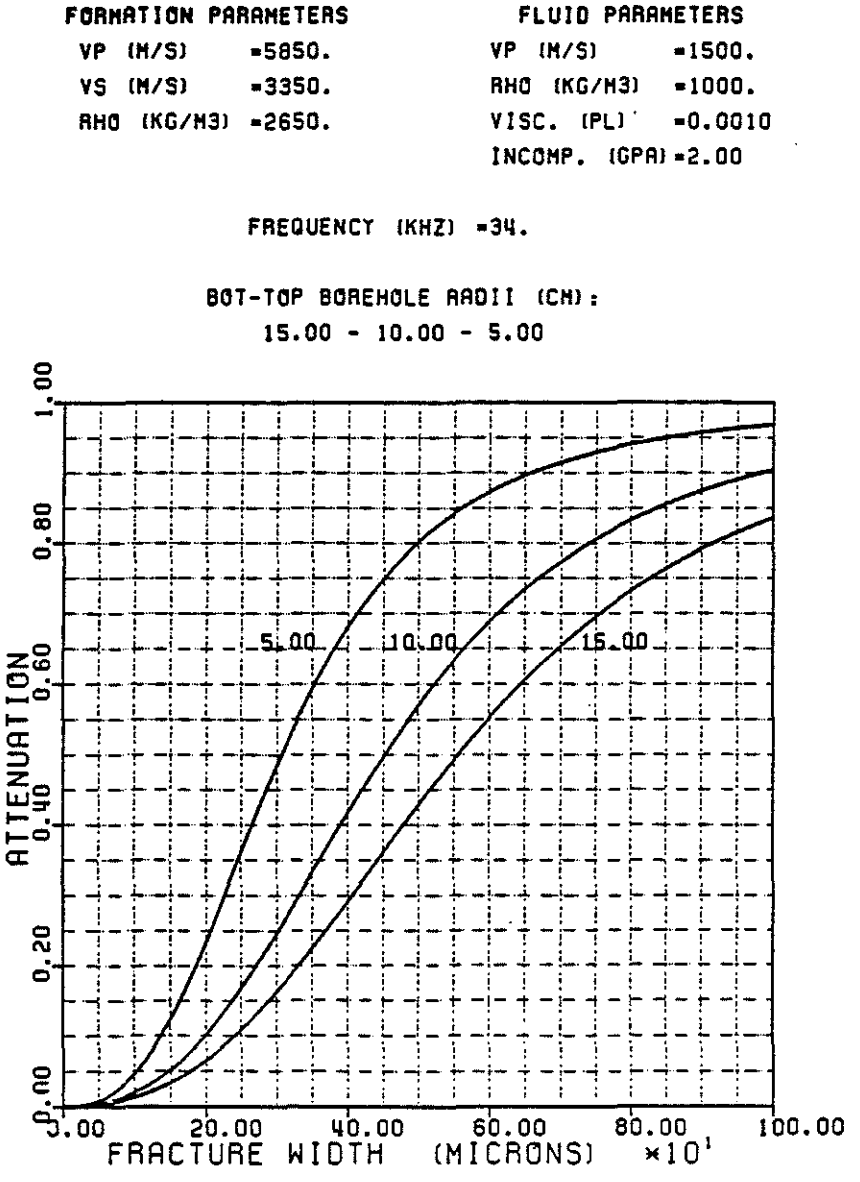

Figure 5b: Borehole radius effect on attenuation in the case of a single fracture.

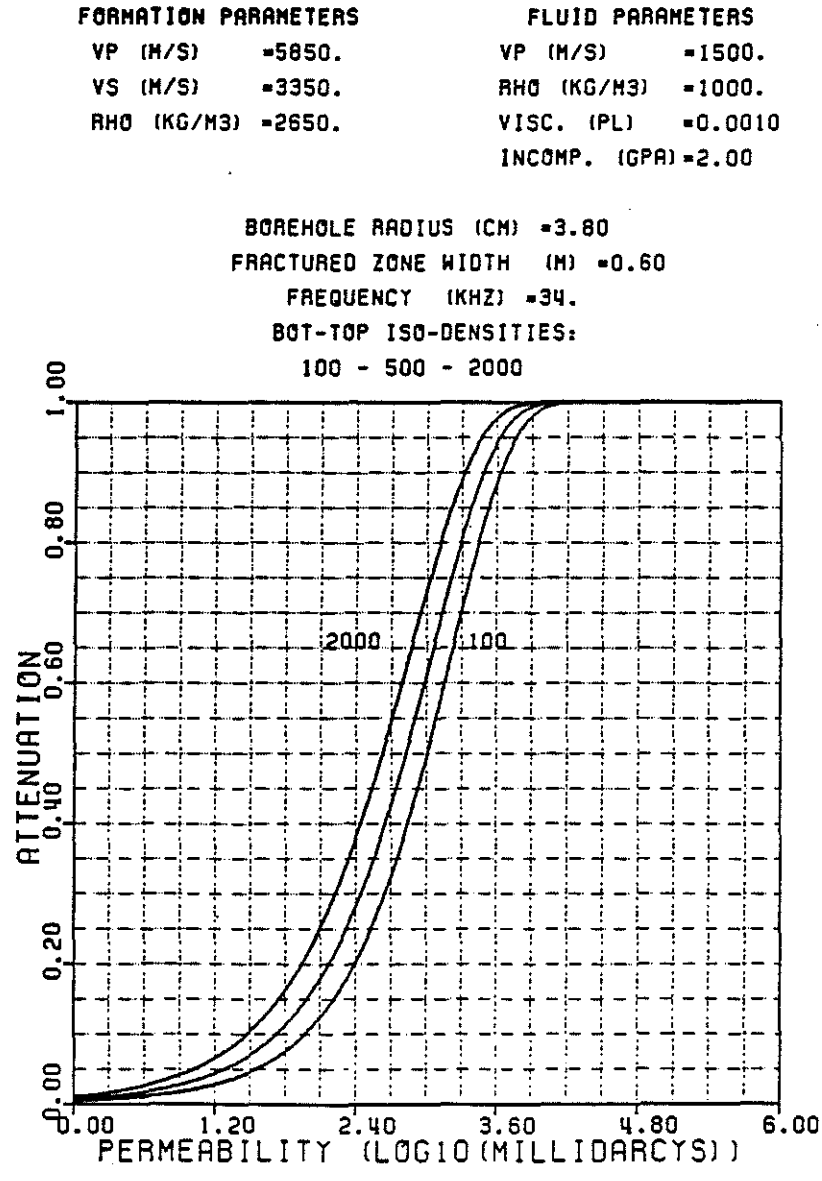

Figure 6: Attenuation versus permeability in the case of a fractured zone.

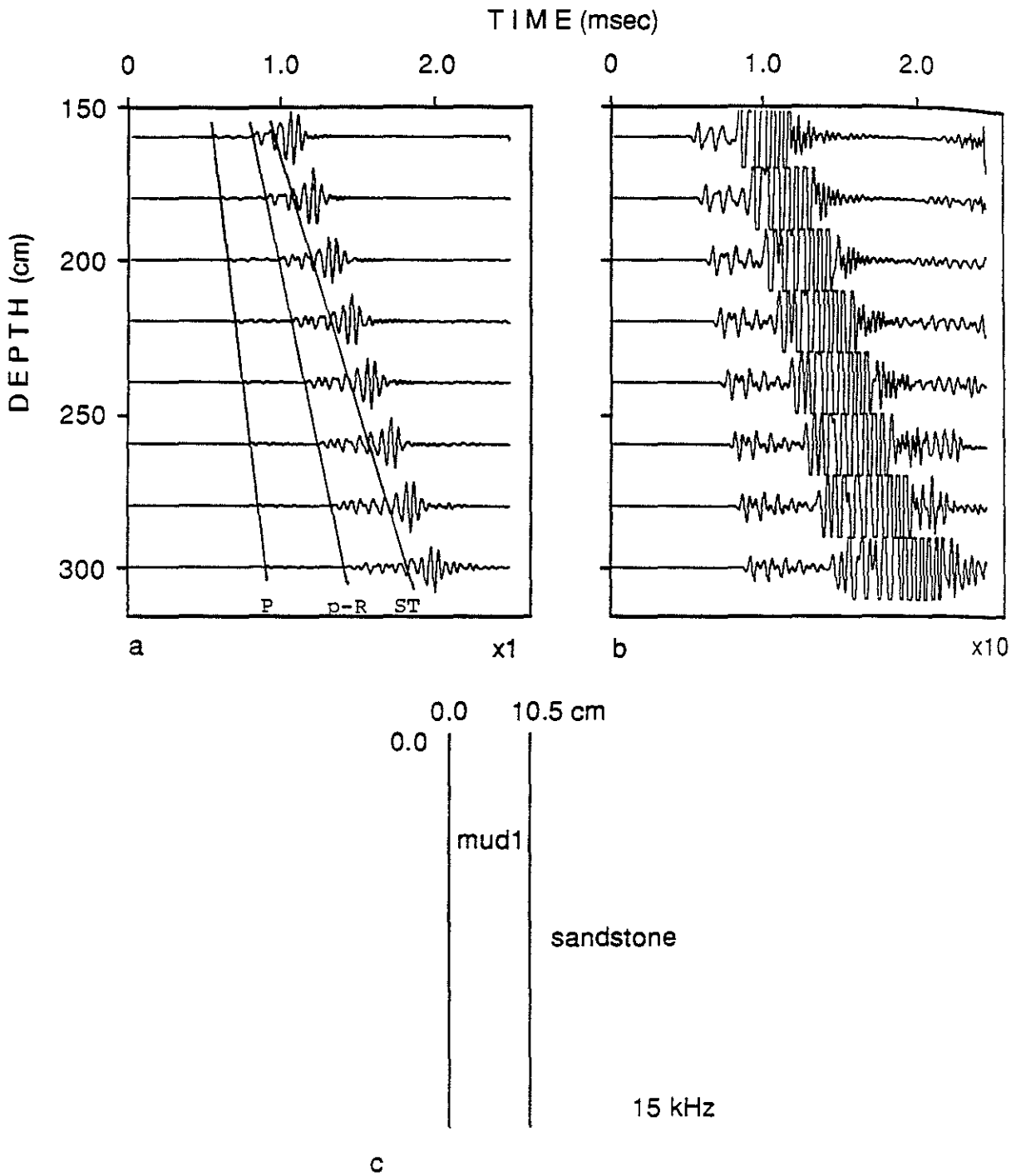

Figure 7a: Synthetic full waveform acoustic log for a vertically homogeneous sandstone.

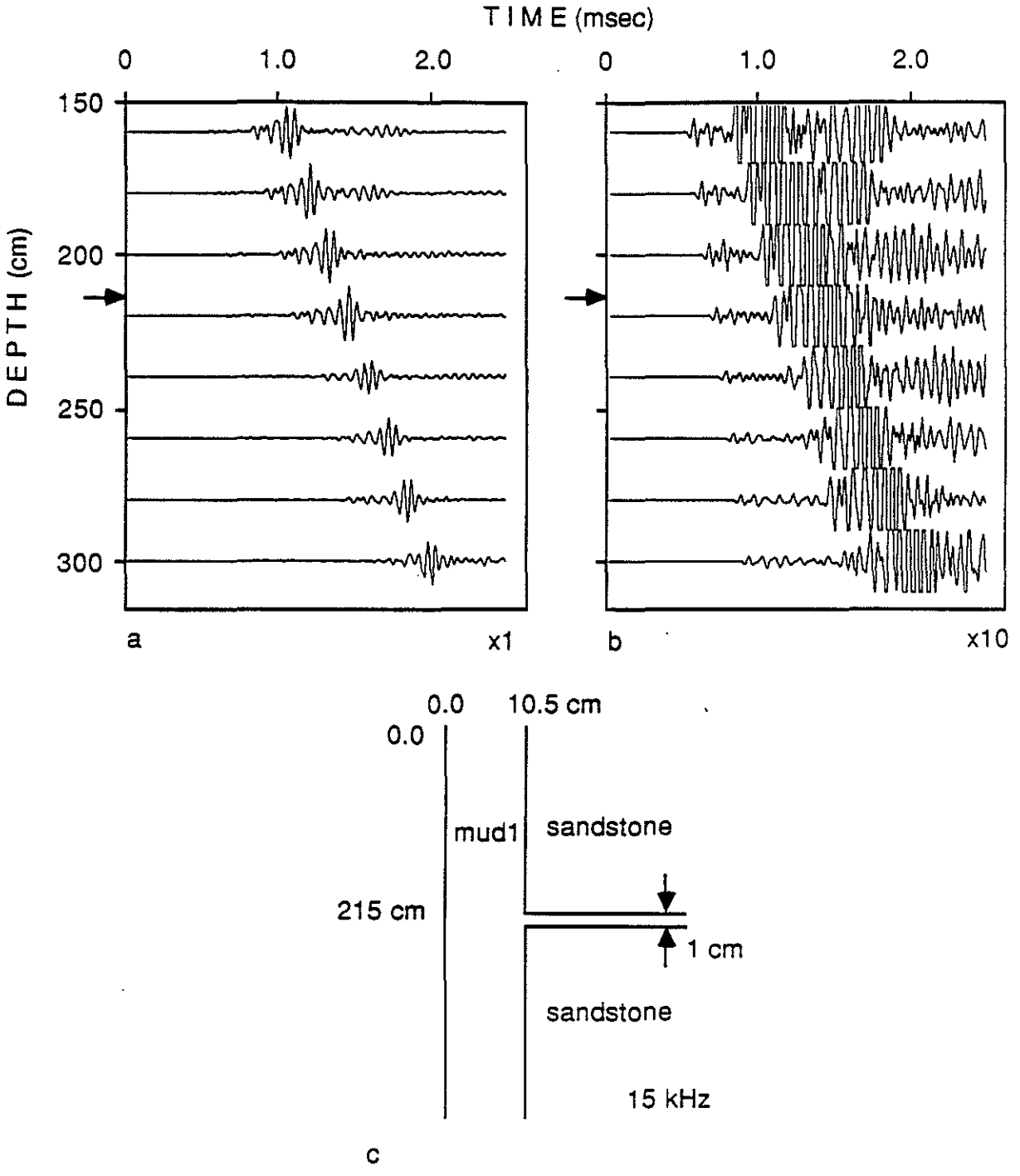

Figure 7b: Synthetic full waveform acoustic log for a 1 cm thick horizontal fissure.

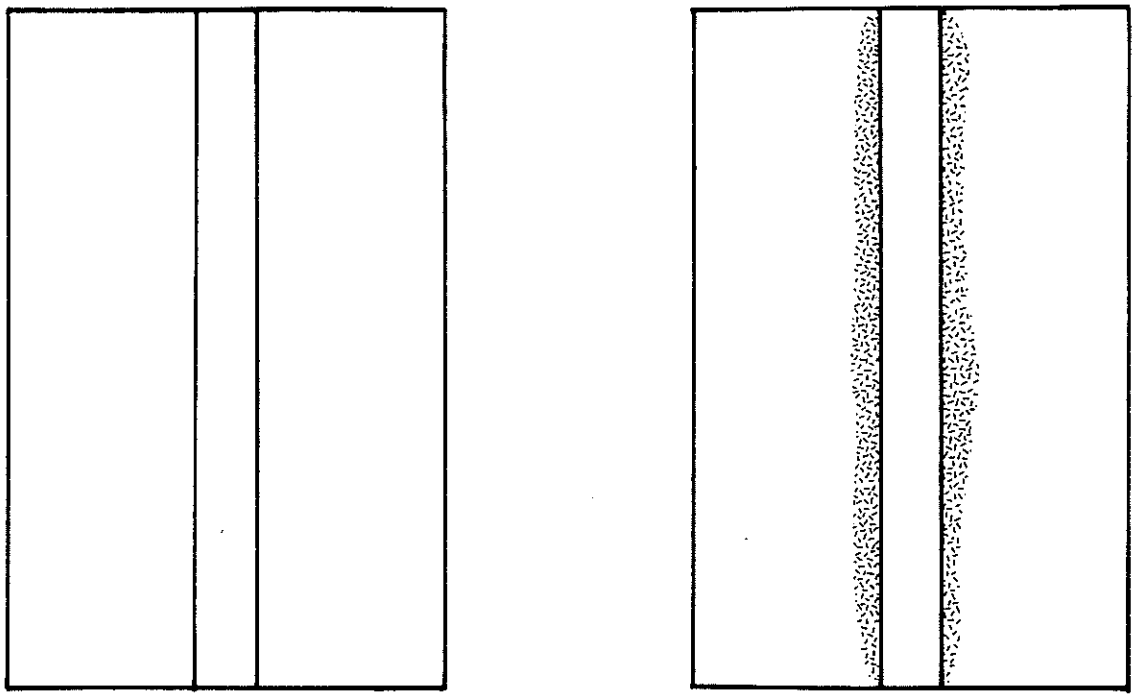

Figure 8: Schematic diagrams of borehole in Lucite: intact (left) and microfractured (right).

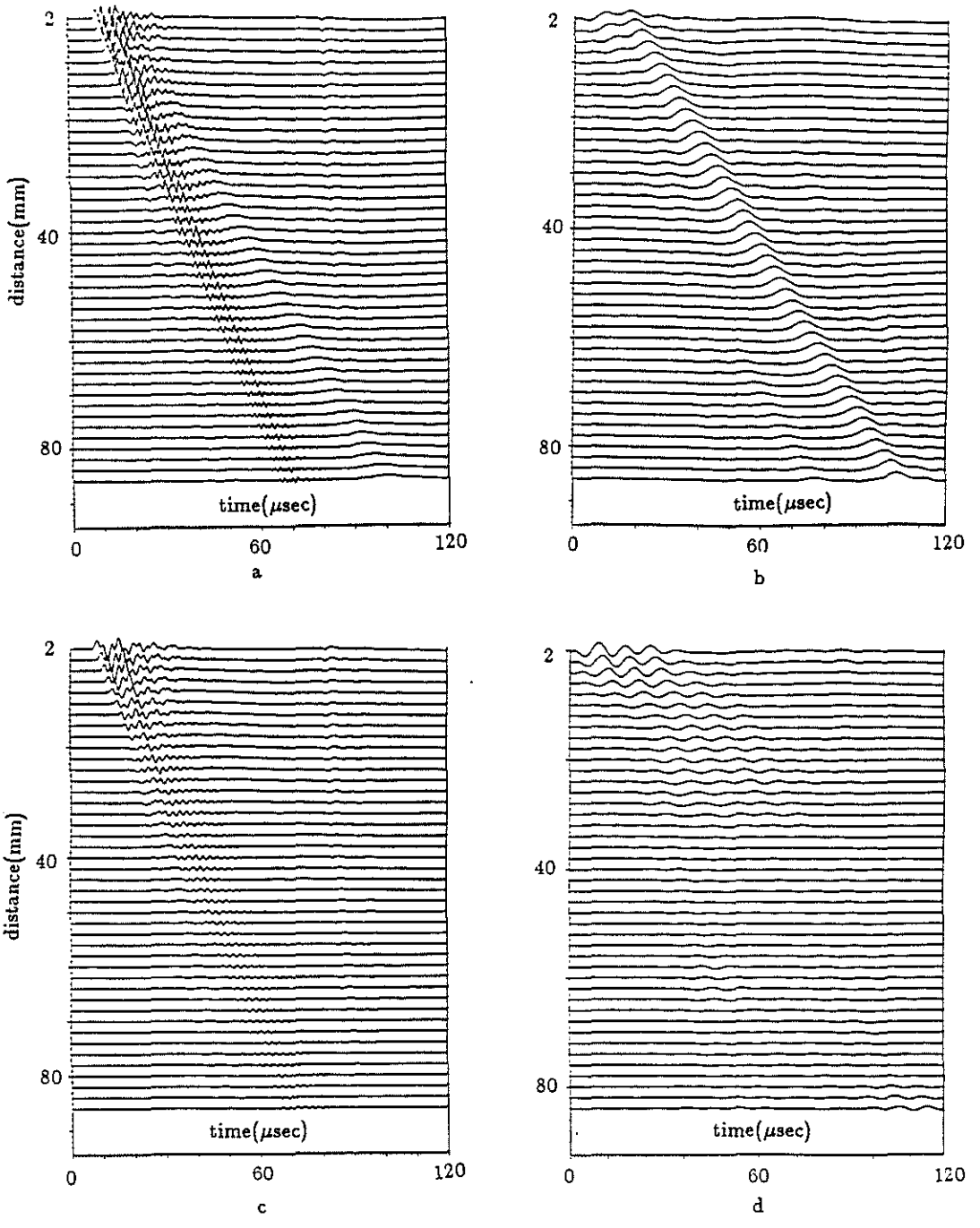

Figure 9: Broadband microseismograms (left) and Stoneley waves (right) recorded in a borehole in Lucite. Top: without microcracks around the borehole. Bottom: with microcracks around the borehole.

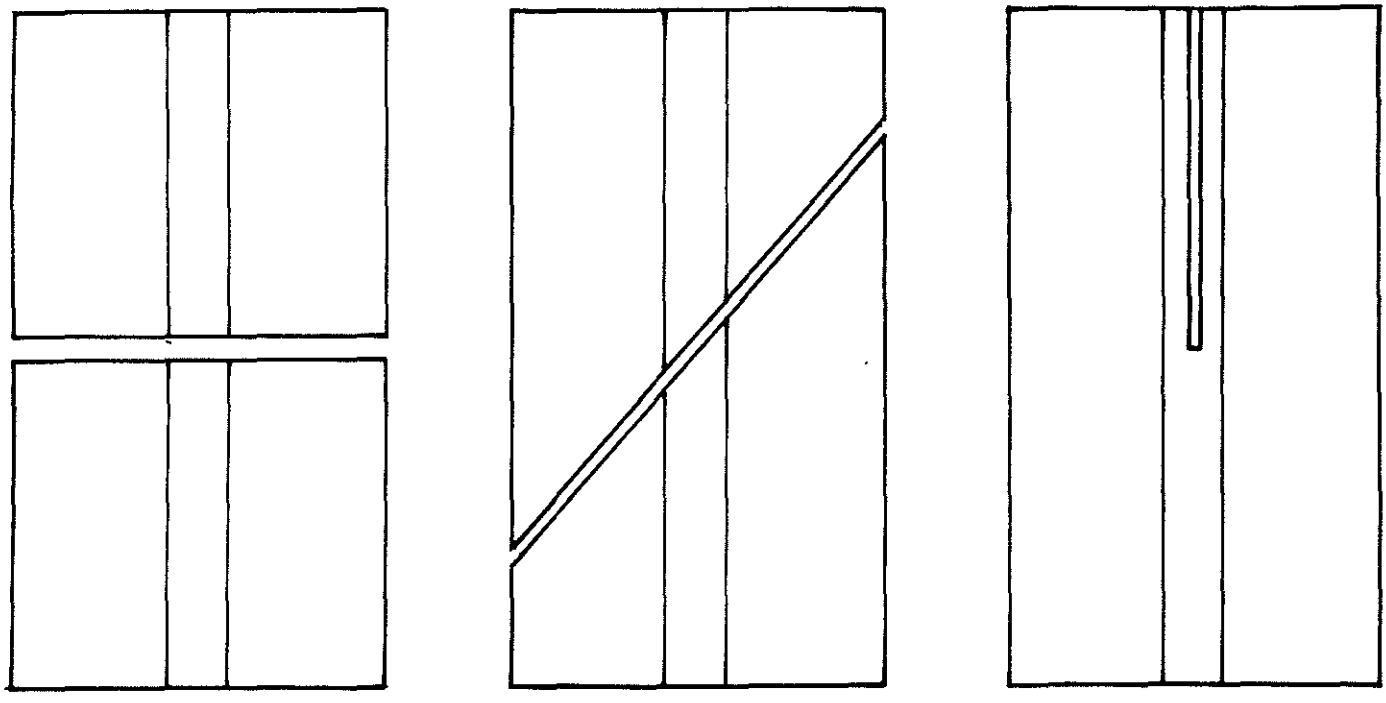

Figure 10: Schematic diagrams of aluminum models with single isolated fractures. Left: horizontal fracture. Middle: fracture inclined at 45°. Right: vertical fracture.

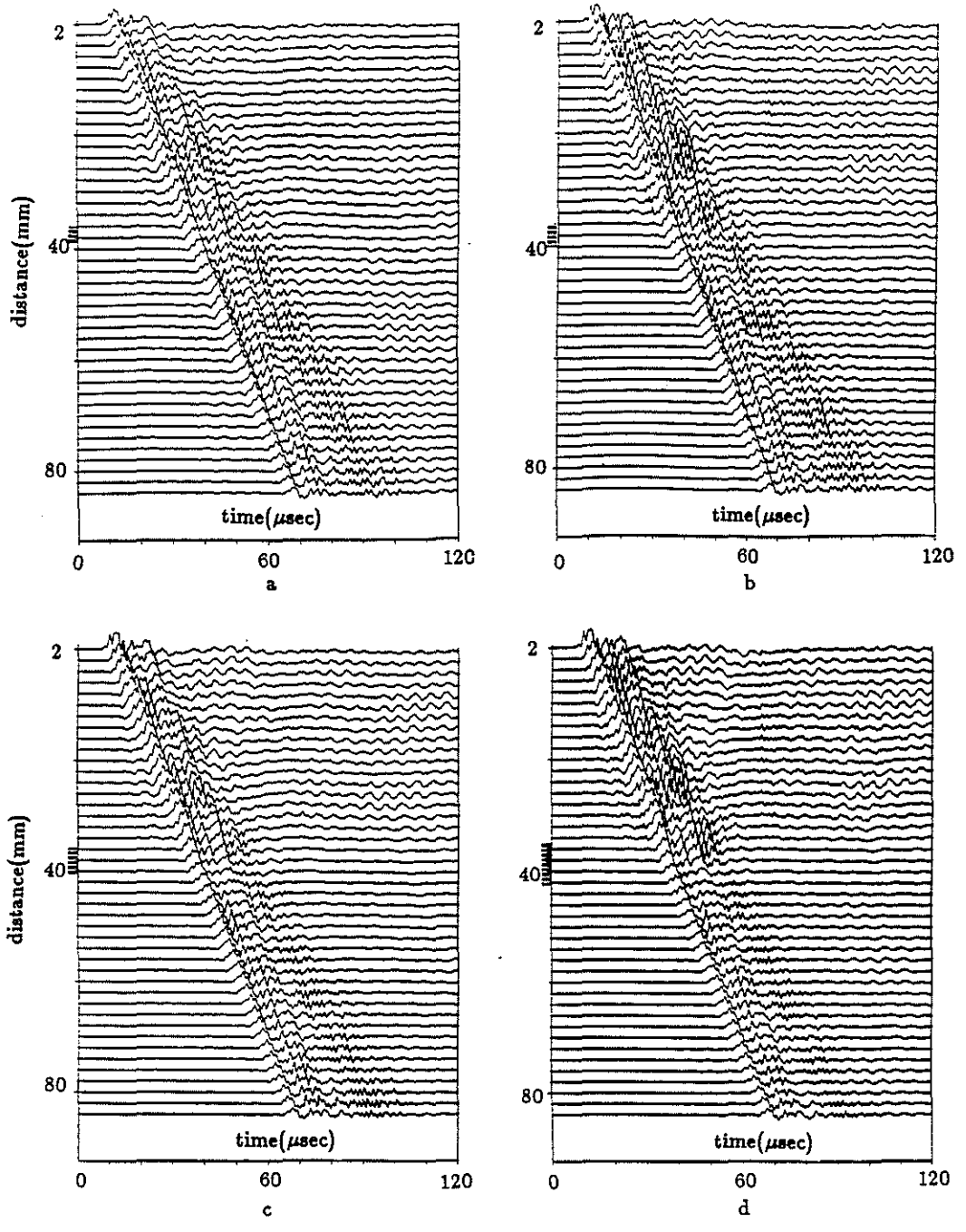

Figure 11: Broadband microseismograms of full waveform acoustic logs as a function of increasing source-receiver distance. A horizontal fracture intersects the borehole as indicated on the vertical axis. Fracture width: (a) 0.2 mm; (b) 1.0 mm; (c) 2.5 mm; (d) 4.5 mm.

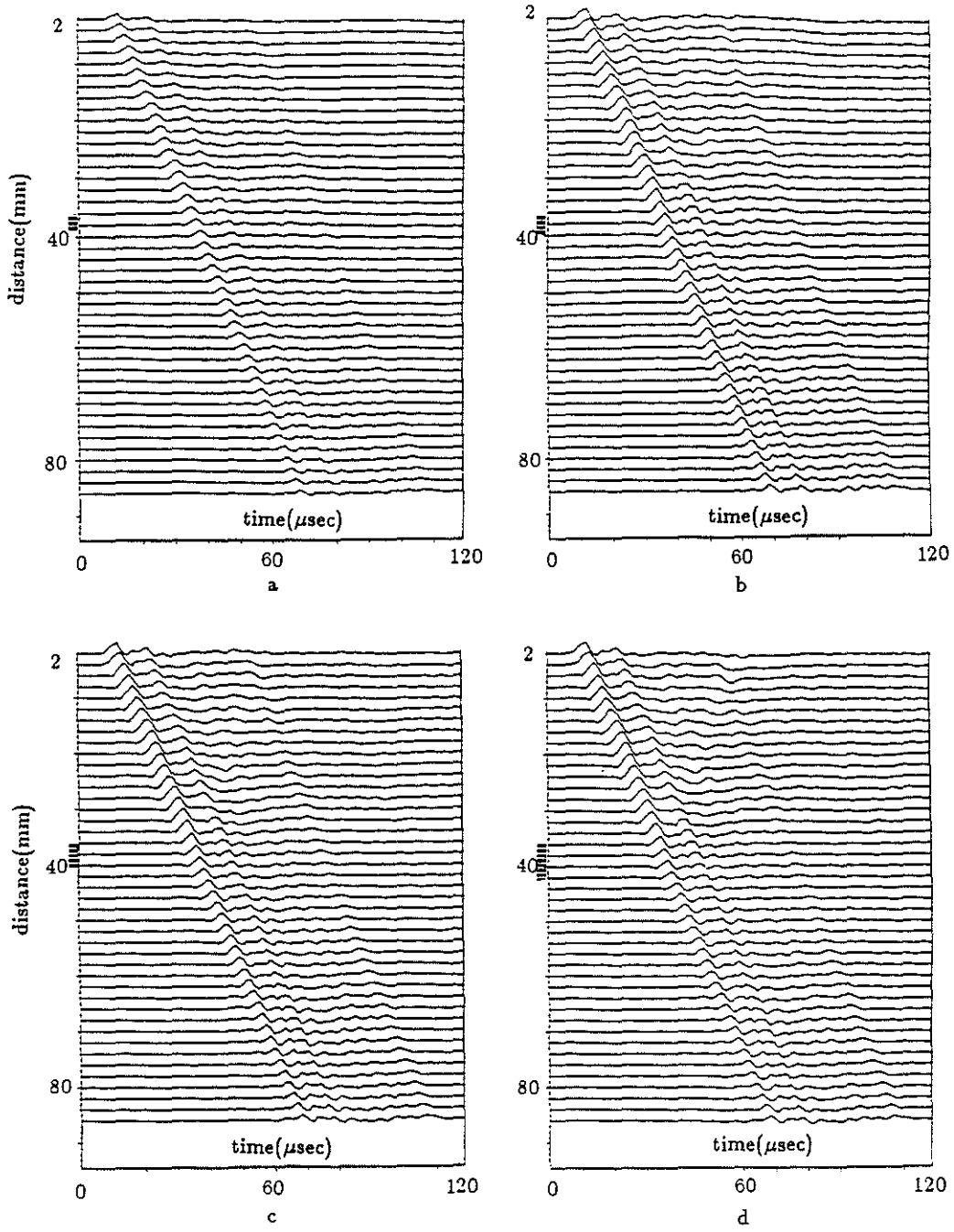

Figure 12: Stoneley waves, obtained from broadband microseismograms by f-k filtering, crossing a horizontal fracture. Fracture is indicated on the left vertical axis. Fracture width: (a) 0.2 mm; (b) 1.0 mm; (c) 2.5 mm; (d) 4.5 mm.

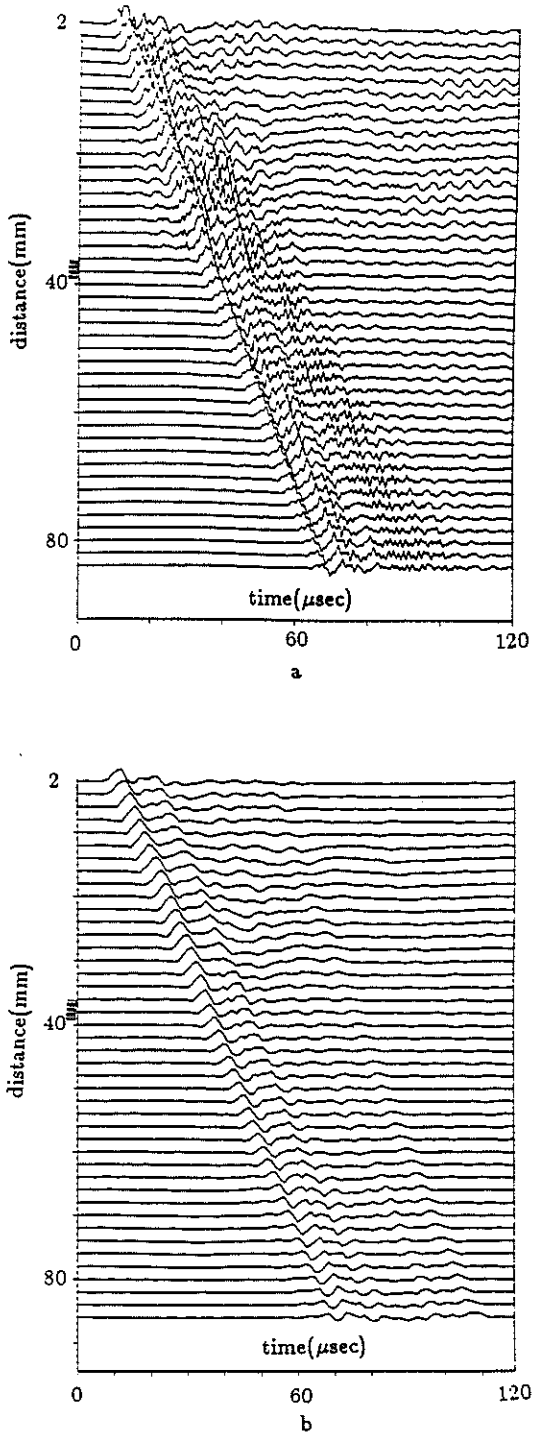

Figure 13: Broadband microseismogram and filtered Stoneley waves in a borehole with a 0.5 mm horizontal fracture.

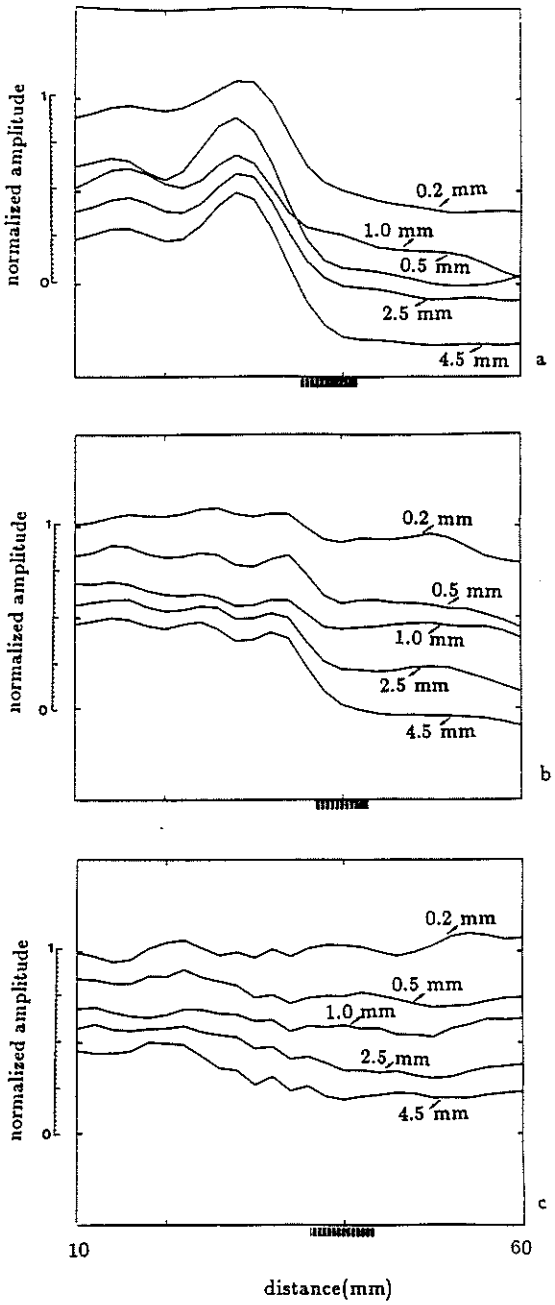

Figure 14: Amplitudes of Stoneley waves as a function of distance along the borehole with a horizontal fracture. Fracture widths are shown on each curve. The curves are shifted vertically to separate them. The amplitude axis is on the left. The fracture is shown at the bottom axis. The three figures are for three different frequency bands centered at: (a) $f_c = 35$ kHz; (b) $f_c = 85$ kHz; (c) $f_c = 135$ kHz.

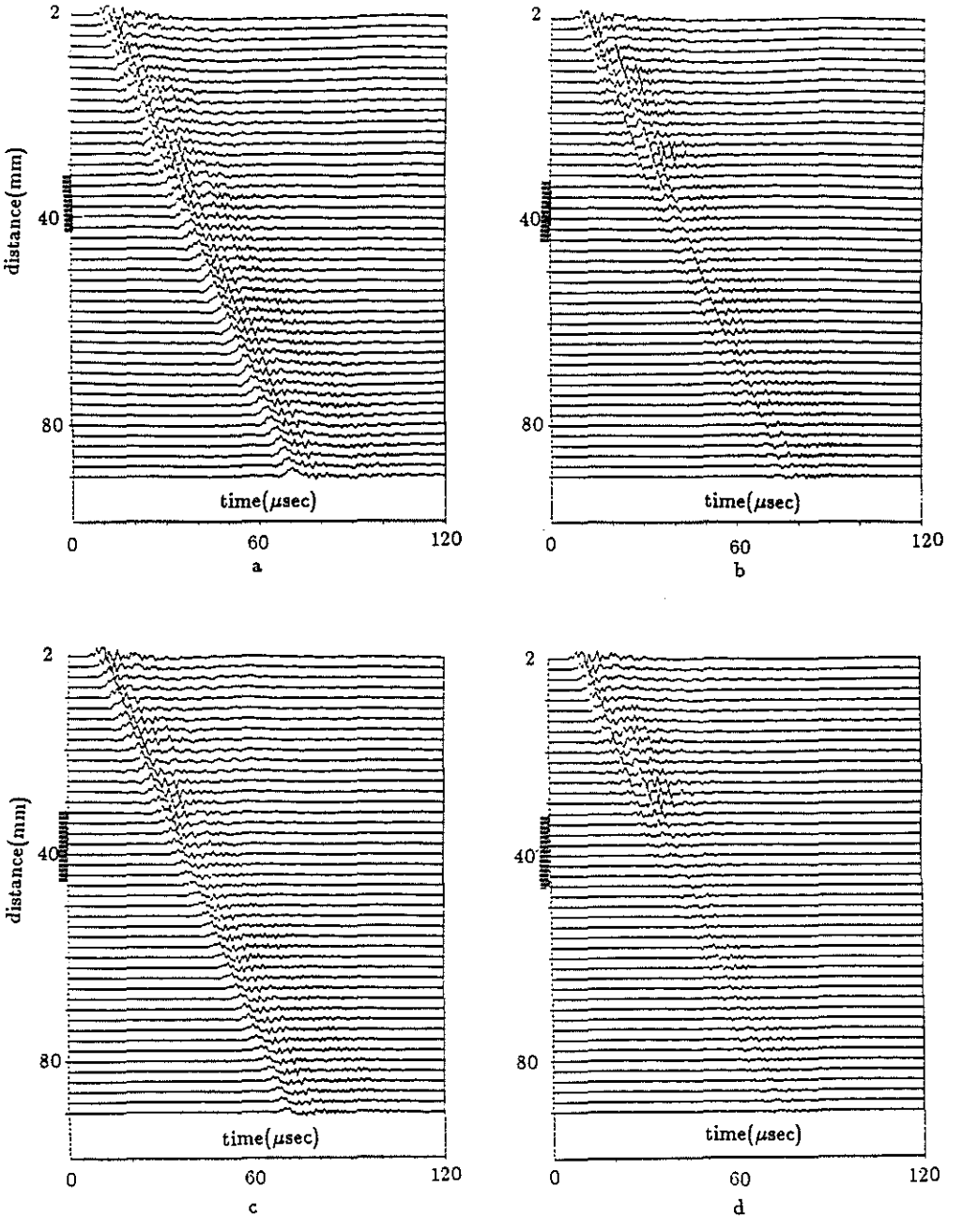

Figure 15: Broadband microseismograms of full waveform acoustic logs in a borehole intersected by a 45°inclined fracture. Fracture width: (a) 0.01 mm; (b) 1.0 mm; (c) 2.5 mm; (d) 4.5 mm.

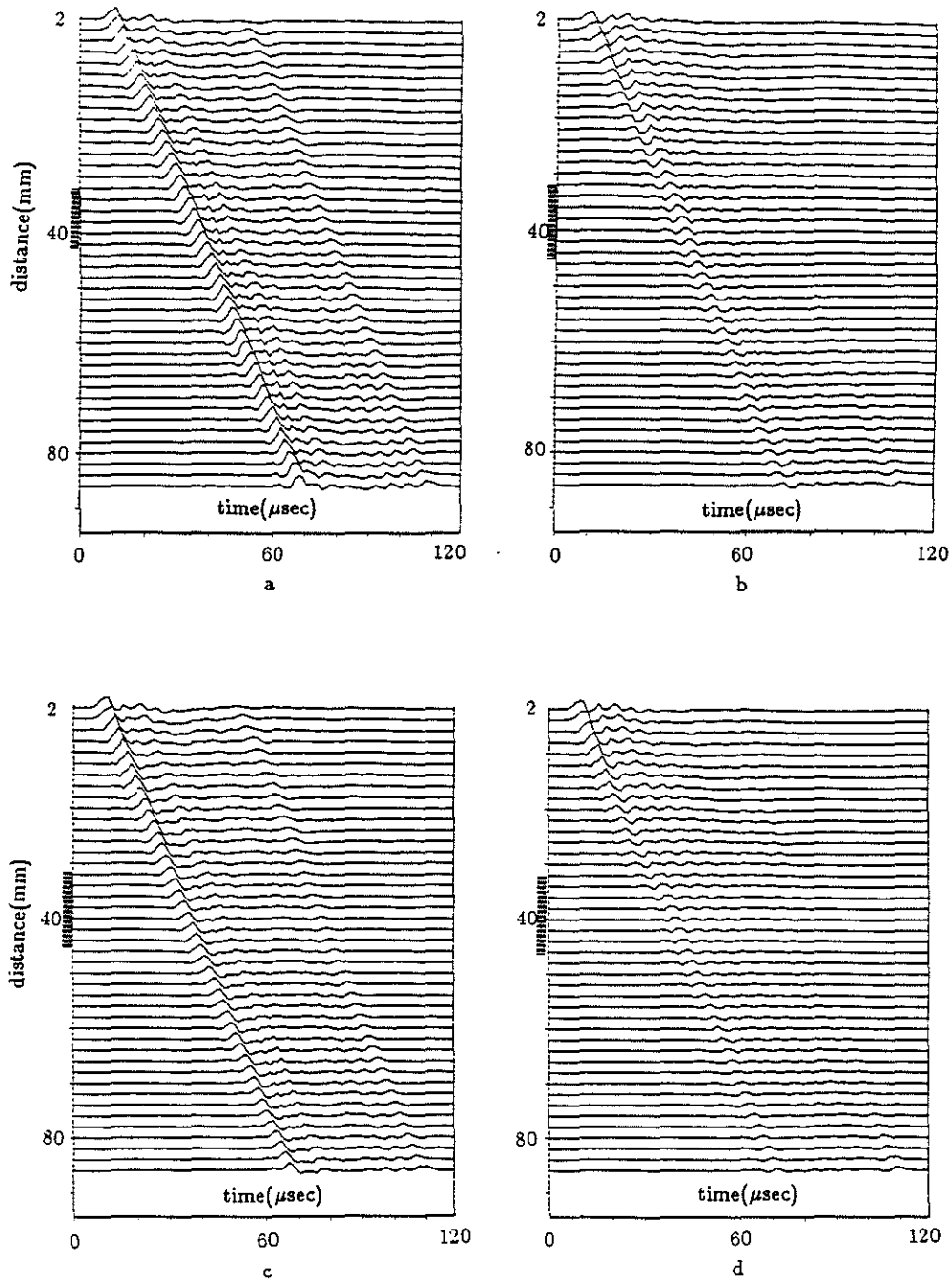

Figure 16: Stoneley waves separated from microseismograms in Figure 15 by f-k filtering. Inclined fracture with thickness (a) 0.01 mm; (b) 1.0 mm; (c) 2.5 mm; (d) 4.5 mm.

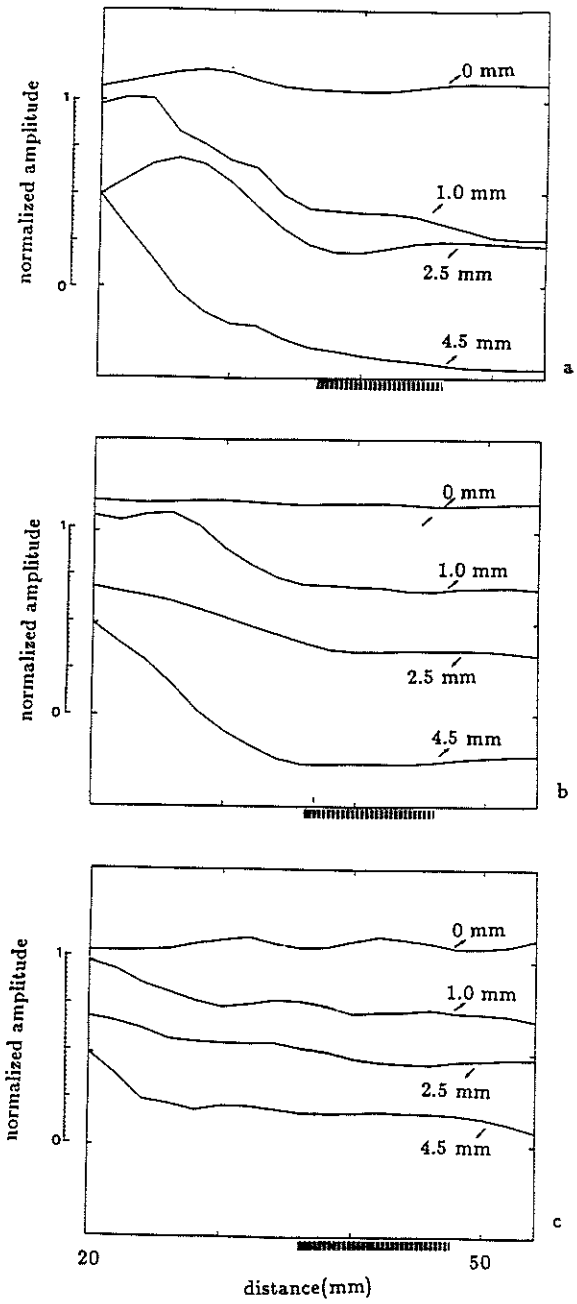

Figure 17: Stoneley amplitudes as a function of distance at three frequency bands for an inclined fracture. (a) $f_c = 35$ kHz; (b) $f_c = 85$ kHz; (c) $f_c = 137.5$ kHz.

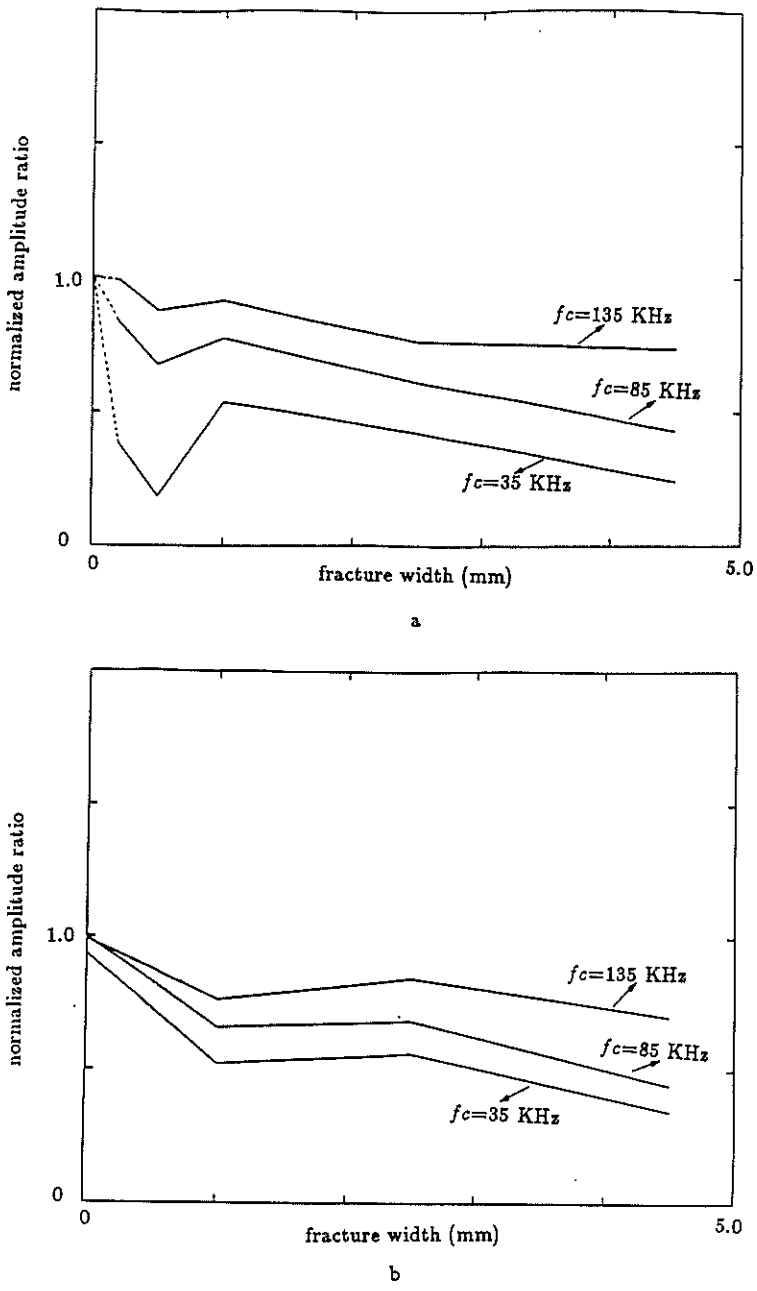

Figure 18: Normalized amplitudes of Stoneley waves as a function of fracture width. Center frequencies are 35, 85,and 135 kHz. (a) horizontal fracture; (b) inclined fracture.

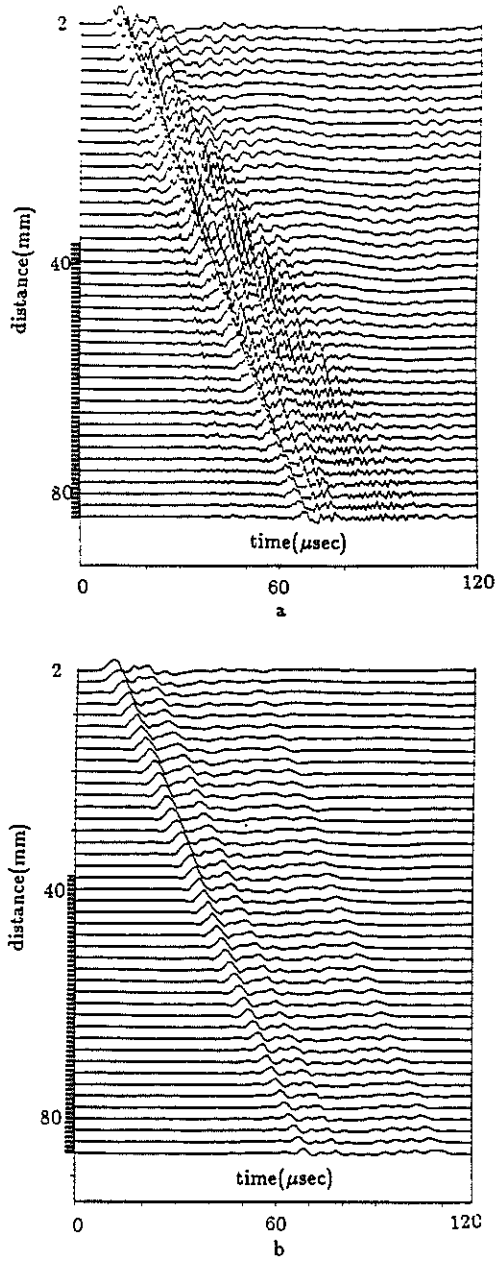

Figure 19: Broadband (top) and Stoneley waves (bottom) microseismograms of full waveform acoustic logs in a borehole with a vertical fracture. Fracture is indicated along the vertical axis on the left.

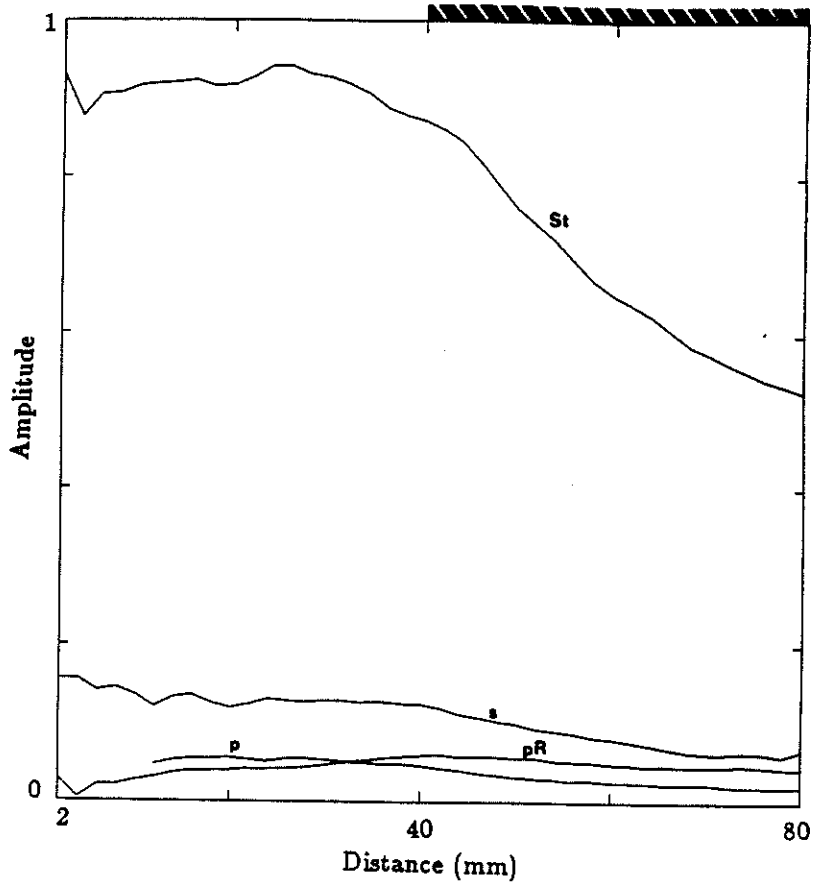

Figure 20: Actual amplitudes of the waves versus source-receiver separation in a vertical fracture extending from 38 mm to 86 mm indicated on the right-hand axis. The fracture width is 1.0 mm. Amplitudes are peak-to-peak maximum amplitudes except for the pseudo-Rayleigh waves, which are RMS amplitudes. Note that the major differences in amplitudes occur in the Stoneley waves (St) which decrease along the fracture. The pseudo-Rayleigh wave (pR) amplitudes increase in the fractured zone due to energy scattering from the Stoneley waves.

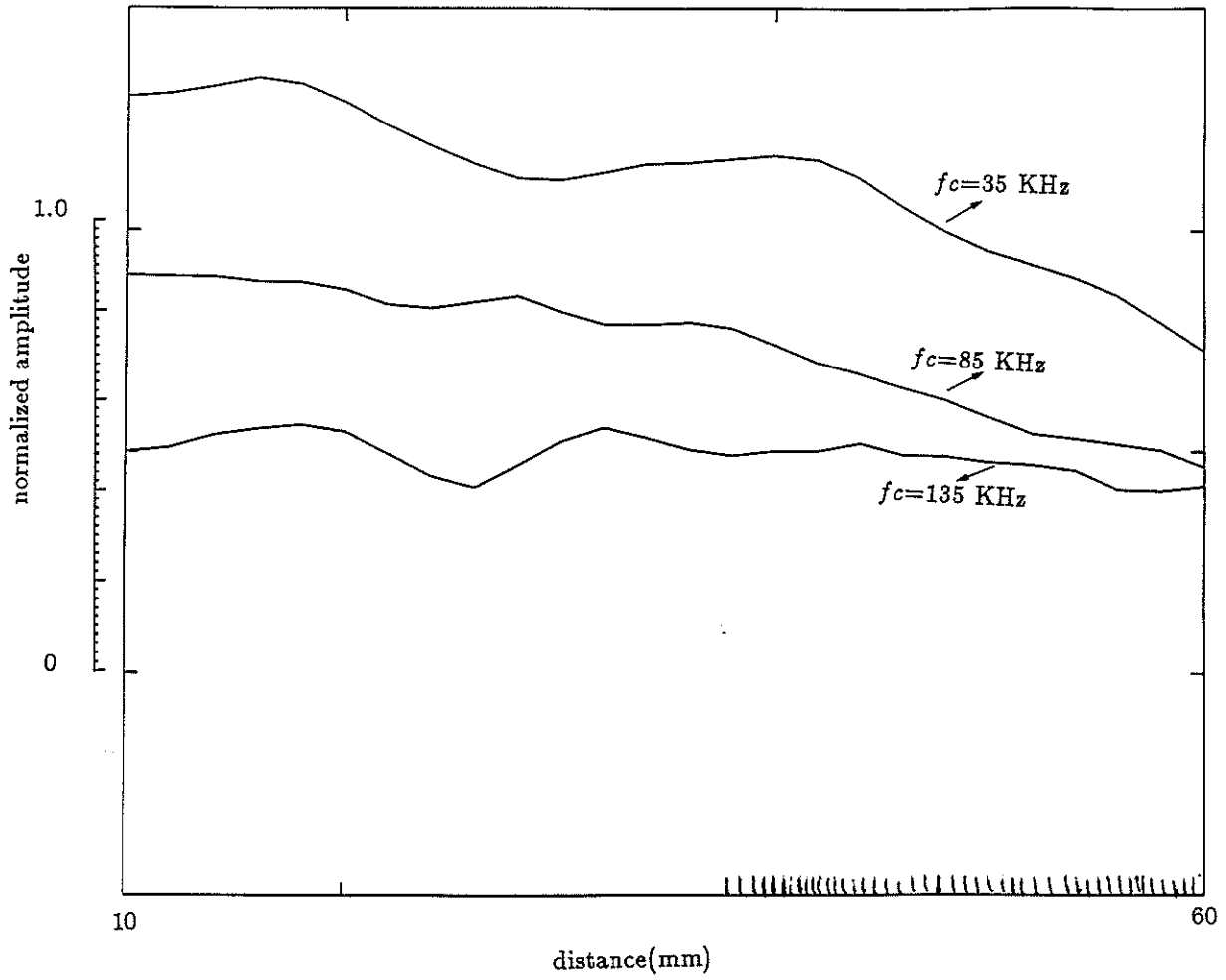

Figure 21: Stoneley wave amplitude in a borehole with vertical fracture at three frequency bands. The fracture is indicated by hatch marks along the x-axis.